City, University of London Institutional Repository

BEHAVIOR OF FRP-STRENGTHENED RC ELEMENTS SUBJECTED TO PURE SHEAR

Mehdi Zomorodian[1], Guang Yang [2], Abdeldjelil Belarbi[3*], Ph.D., P.E., Ashraf Ayoub[4]

[1]Structural Engineer, Matrix Structural Engineers, Houston, USA. E-mail: mzomorodian@matrixstructural.com

[2]Graduate Engineer, Walter P Moore and Associates, Houston, USA. E-mail: gyang@walterpmoore.com

[3*]Hugh Roy and Lillie Cranz Cullen Distinguished Professor, Department of Civil and Environmental Engineering, University of Houston, Houston, USA. E-mail: belarbi@uh.edu

[4]Professor, City, University of London. E-mail: Ashraf.Ayoub.1@city.ac.uk

ABSTRACT

The shear behavior of fiber reinforced polymer strengthened reinforce concrete (FRP strengthened RC) has been the focus of extensive research studies. However, the mechanism of this complex phenomenon has not been fully clarified. Recent analytical models which were developed for predicting the shear capacity of FRP strengthened RC girders were based on test results of simply supported beam specimens with various shear span-to-depth ratios. In such tests no region of the specimen is subjected to uniform stress conditions, Therefore, the results of such tests cannot predict the true pure shear behavior due to non-uniformity of stresses, the presence of flexural and other non-shear related effects such as a/d ratio that cannot be filtered out. Therefore, proper design of shear strengthening using FRP requires testing of elements that are subjected to pure shear case primary before adding other governing effects. This allows a careful investigation and full understanding of the behavior at the element level. In order to accomplish this task, panel testing of representative RC specimens strengthened with FRP sheets were needed. This paper reports the testing of 10 FRP strengthened RC panels subjected to pure shear stress field. The tests were carried out to evaluate the effects of three

27 variables: FRP stiffness, FRP wrapping scheme, and transverse steel reinforcement ratio. The

28 test results showed that these three variables greatly affected the shear behavior due to various

29 types of failure modes associated with FRP strengthening. In addition, it was observed that the

30 magnitude of increased shear capacity associated with the application of FRP sheets depends not

31 only upon the stiffness of FRP, but also on the stiffness of internal shear reinforcement. With the

32 increase of internal steel shear reinforcement, the effectiveness of shear gain due to externally

33 bonded FRP decreases.

34 Keywords: Shear behavior; FRP strengthened RC members; Failure modes; Wrapping Scheme

35
36 **INTRODUCTION**

37   As a response to corrosion problems in reinforcing steel, and to increase the efficiency of

38 strengthening systems in terms of time and ease of application, FRP composites have been

39 increasingly used in rehabilitation and strengthening of RC structures [1]. The complex behavior

40 of FRP-strengthened RC structures with predominant shear behavior has been previously studied

41 through extensive experimental and analytical investigations [2-4]. Research related to the

42 flexural behavior of FRP-strengthened elements has reached an advanced stage, and well

43 established analytical models are available for analyzing and designing FRP-strengthened beams

44 and columns under flexural and axial-confinement actions [1, 5]. However, the experimental and

45 analytical research related to FRP strengthened RC under shear load are limited and has not been

46 fully developed [6-10]

47   To predict the behavior of FRP-strengthened RC elements in shear, the truss model

48 approach is commonly utilized by researchers [8, 11-12]. In the truss model analogy, constitutive

49 laws of each component, namely concrete, steel, and FRP external reinforcement are crucial for

50   acceptable predictions. The results presented in this paper are part of a research work which

51   aimed at developing a modified softening membrane model (SMM) for FRP-strengthened RC

52   elements subjected to shear stress field. The SMM is based on a truss model and has been

53   developed and was used to predict the entire shear stress-strain curve of the RC element under in-

54   plane shear stress field [13]. The materials laws utilized is SMM was a work carried out by

55   Belarbi et al. [14] and are widely accepted and used in several versions of the Softened truss

56   models [13,15]. While adding external reinforcement such as FRP sheets, the behavior of

57   elements such as concrete, steel and FRP are typically altered due to several effects such as the

58   crack pattern, softened concrete struts, and Poison's ratio. The smeared stress-strain behavior of

59   the constituents of strengthened member including concrete and reinforcing steel will be

60   fundamentally different than their corresponding values for un-strengthened specimens.

61   Consequently, different failure modes exist, and in turn affects the shear strength. In addition to

62   the failure modes related to concrete in RC members such as diagonal tension failure in the

63   web, shear compression failure in compression zone and flexure failure, FRP

64   debonding and FRP rupture are common failure modes in FRP strengthened RC

65   members [4, 11]. The problem is further complicated due to the presence of several additional

66   parameters that might influence the behavior; parameters such as the properties of the FRP

67   material, the angle of fiber direction, the characteristics of the fiber-resin interface and FRP-

68   concrete interface, the presence of mechanical anchors, and the use of FRP strips as opposed to

69   continuous sheets. These additional parameters modify the crack patterns, failure modes, and in

70   turn influence the constitutive behavior of concrete [6,8,16]. Recent analytical models that were

71   developed for predicting the shear capacity of FRP-strengthened RC beams are based on test

72   results of simply supported beam specimens with various shear span-to-depth ratios. Results of

3

73   such tests cannot represent the true pure shear behavior due to the presence of flexural and other

74   non-shear related effects that cannot be filtered out. As a result, a rational shear design cannot be

75   accurately developed. An efficient method to evaluate the overall shear response of a member is

76   to identify the characteristic behavior and the contribution of each element and material

77   constituting the structure [17]. Reinforced concrete structures, such as shells and nuclear

78   containment vessels, resist applied loads primarily through in-plane stresses. Each structure can

79   be characterized as an assembly of elements, each subjected to two in-plane normal stresses and

80   one in-plane shear stress [18]. To perform a rational analysis and thoroughly understand the

81   behavior of FRP-strengthened RC structures, elements (panels) are isolated from the structure.

82   Once a rational model is developed to predict the shear behavior in element level, the model can

83   then be incorporated into a finite element program to predict the behavior of the whole structure.

84   The first step in the research was to experimentally investigate the shear constitutive behavior of

85   FRP-strengthened RC elements subjected to pure shear. To evaluate such behavior, a series of

86   full scale FRP-strengthened RC panels were constructed and tested using the Universal Panel

87   Tester housed at the University of Houston [17]. Pure shear loading condition was simulated

88   through proportionally applied biaxial tension-compression load. The test results of 10 elements

89   (panels) subjected to pure shear loading are reported in this paper. The second step of the

90   research was to develop an analytical model to predict the behavior of FRP-strengthened RC

91   membrane elements subjected to pure shear. This new model, so-called the Softened Membrane

92   Model for FRP-strengthened RC members (SMM-FRP), is described elsewhere [16,19].

93   The shear behavior of FRP-strengthened RC members is influenced by various factors. This

94   study focuses on parameters that have been recognized by other researchers to have the most

95   influence on the behavior [6,8,20]. These parameters are (1) FRP reinforcement ratio (FRP

96   stiffness), (2) wrapping scheme, and (3) transverse steel reinforcement ratio.

FRP Sheet Stiffness

98   FRP sheet stiffness $(E_f t_f)$ affects the contribution of FRP reinforcement to the overall

99   shear strength of FRP strengthened RC members. Previous research studies have indicated that

100   there exists a limit with respect to axial rigidity of the applied materials beyond which no

101   increase in shear capacity is expected [20]. When the thickness of the FRP sheets applied to RC

102   beam increases, the ultimate shear strength gain is limited by premature debonding from the

103   concrete substrate [21]. Also, the disproportionate strength gain when the FRP thickness (FRP

104   stiffness) increases is due to the fact that the ultimate failure is primarily governed by the

105   concrete cracking, splitting and loss of aggregate interlock [4]. Furthermore, as the FRP axial

106   stiffness increases, the effective strains in the sheets decrease [6], therefore, the FRP materials

107   will not reach their expected capacity before failure. In this case, the failure mode of the member

108   will be either concrete crushing or FRP debonding instead of FRP rupture.

109   Design guidelines such as ACI 440.2R-08 [1], CAN/CSA S806-12 [22] and *fib*-TG9.3 Bulletin

110   14 [23] fail to incorporate such behavior for strengthened beams when the thickness of FRP

111   sheets (and hence the stiffness) is high. These design guidelines are based on Triantafillou's [24]

112   statement that contribution to shear strength will increase with low values of axial stiffness.

113   Therefore, only when FRP sheets with low thickness is applied, the current design guidelines are

114   satisfactory [2].

Wrapping Scheme

The wrapping scheme affects the confinement due to the FRP sheets, and the potential for debonding. Common wrapping schemes in shear strengthening are fully wrap, side bond, U-Wrap, and U-wrap with FRP anchor.

The FRP anchor provides an effective way of anchoring the FRP composite to the RC substrate. There have been several studies regarding the design and implementation of FRP anchors [25-28]. The main parameters considered in designing the FRP anchors include the anchor diameter, number of anchors needed and anchor length. The FRP anchor used in this research had a diameter of 12.7 mm and a length of 610 mm as shown in Fig. 3. A contact length of 216 mm was used to cover the whole width of the FRP sheets with 6.5 mm extra on both sides, which satisfies the recommended length suggested by Kobayashi et al. [29].

Transverse Steel Reinforcement Ratio

Previous studies have revealed that the magnitude of increased shear capacity associated with the application of FRP materials depend not only upon the type of FRP that is being used, but also on the amount of internal shear reinforcement [8,21,30]. Researchers have indicated that the contribution of FRP in shear gain reduces when the beam is heavily reinforced in shear. This is because the maximum shear contributions of steel stirrups and FRP material may not be reached simultaneously. Also, with the increase of steel shear reinforcement, the measured effective strain reduces [6].

EXPERIMENTAL PROGRAM

In order to evaluate the shear behavior of FRP-strengthened RC members and to investigate the main factors that influence the behavior of such members, full-scale tests of 8 FRP-strengthened RC panels and 2 un-strengthened RC control panels were conducted.

138 The test panels were 1397×1397×178 mm (55×55×7 inches) in size, as shown in Fig. 1. The

139 longitudinal and transverse steel reinforcements were arranged at a 45 degree angle with respect

140 to the principal directions of the applied loads (1-2 coordinates) along l and t directions and the

141 external FRP reinforcement was applied along transverse (t) direction. The steel reinforcement

142 was grade 60 deformed bars with cross-sectional areas of 71 mm^2 (#3 rebar) and 129 mm^2 (#4

143 rebar) spaced at 188 mm in both longitudinal and transverse directions. The FRP sheets utilized

144 in the experimental program which are typically used for shear strengthening in practice, consist

145 of unidirectional carbon fibers attached on the two opposite surfaces of the panel specimens. The

146 overall FRP sheet layout of the specimens is shown in Fig. 2a. The FRP strips had a width of 144

147 mm, and 188 mm center to center distance. The nominal strength of concrete was 52 MPa. The

148 rebar was welded onto a pre-embedded connector inserts that were connected to the loading

149 actuators by high-strength bolts. The steel reinforcement ratios and FRP sheet thicknesses were

150 chosen carefully in order to study the effect of FRP stiffness on the shear behavior and also the

151 effect of the ratio of FRP reinforcement to steel reinforcement. Three common wrapping

152 schemes in shear strengthening are adopted, namely, 1) fully wrap, (2) side bond, and (3) U-wrap

153 with FRP anchor. The fully wrap is to ensure that debonding is eliminated and the FRP will

154 reach its ultimate strength, while the side bonding scheme is to evaluate the behavior up to FRP

155 debonding occurs. The U-wrap with FRP anchor is to simulate the real case of shear

156 strengthening with FRP in T-beams, where fully wrap method is infeasible due to the flanges.

157 Fully wrap and side bonding wrapping scheme of the panels are shown in Fig. 2b and Fig.2c,

158 respectively. Details of the U-wrap with FRP anchor are given in Fig. 3.

159 The test matrix in the experimental program is shown in Table 1. The specimens are identified

160 using transverse rebar size (No.3 and 4), FRP thickness [0.6, 1 mm, and 2 mm (0.025, 0.040 and

161   0.080 inch)] and wrapping schemes, namely, Fully Wrap (FW) (Fig. 2b), Side Bond (SB) (Fig.

162   2c), and U-wrap with FRP Anchor (FA) (Fig. 3). As an example, P4-025-SB stands for the

163   specimen with #4 transverse rebar, 0.6 mm (0.025 in.) thick FRP sheets and side bond (SB)

164   wrapping scheme. REF-P3 and REF-P4, stand for RC reference specimens with No. 3 and 4

165   transverse rebar, respectively.

166   Standard material tests were conducted to obtain the material properties. Type III cement was

167   used for concrete casting. Standard 152 mm × 305 mm (6 x 12 inch) cylinders were tested to

168   obtain the compressive strength of concrete $f_c^{'}$ as per ASTM C39 [31]. The FRP sheets were

169   made of unidirectional carbon fibers with the material properties determined from coupon tests

170   per ASTM D3039 [32]. The wet lay-up system was used for installation of FRP sheets. The

171   specimen was ground, sandblasted, and power-washed to provide the proper concrete surface

172   conditions that would develop the necessary bond strength between the concrete and FRP sheets.

173   Putty and primer were first applied on the surface; the sheets were then impregnated with epoxy

174   resin and applied in-situ. Specimens were then cured for a minimum of 72 hours before testing. .

175   Along with preparing each specimen, a concrete beam was cast and FRP was applied to test the

176   pull-off strength of the FRP-concrete interface. To have a quality control of the bond strength of

177   the FRP-concrete interface, the standard pull-off tests were carried out by using the Dyna Z16

178   pull-off tester. The test follows the requirements of ASTM D7522 [33]. Before the pull-off test,

179   several 2 in. diameter cores were cut by a core drill, then the 2 in. diameter aluminum disks were

180   attached onto the FRP sheets by high strength epoxy, with manufacture tested strength of 1500

181   psi. When testing, the disk was attached to the pull-off tester and the pull-off load was applied by

182   the manual crank. The ultimate load was captured by the load indicator and used to calculate the

183   pull-off strength. The pull-off strength, σ_p shall be at least 1.4 MPa [1]. Details of the respective

184   material properties of steel and FRP are presented in Table 1, where E_{ls} and E_{ts} are the steel

185   modulus of Elasticity in l and t directions, respectively; and E_f are the modulus of elasticity of

186   steel and FRP, respectively; ρ_t and ρ_l are the steel reinforcement ratios in l and t directions,

187   respectively; and f_y is the yielding strength of steel.

188   **Loading Method and Instrumentation**

189   Proportionally applied tensile load (horizontal σ_1) and compressive forces (vertical σ_2)

190   were used to simulate a pure shear loading condition in the experimental test. As shown in Fig. 4,

191   the reference l-t coordinate system represents the directions of longitudinal and transversal

192   reinforcements. The reference 1-2 coordinate system represents the directions of the principal

193   compressive stress (2-axis) and tensile stress (1-axis). Testing initially started using load control

194   with increments of 1 kN/min. up to first cracking and then switched to displacement control

195   with the increment of strain in the horizontal direction set to 0.0001 (mm/mm)/min until the

196   specimen failed.

197   The average (smeared) strains in the horizontal, vertical, and diagonal directions were measured

198   by a total of 14 Linear Variable Differential Transformers (LVDTs) attached on both sides of the

199   panel specimen. With the stable reading from LVDTs, the stress-strain curves of concrete panels

200   in the post peak branches were reliably monitored. On the North side, the panel specimen was

201   instrumented symmetrically by 10 LVDTs. Four of the LVDTs were aligned horizontally, and

202   another set of 4 LVDTs were aligned vertically, and each one of the remaining two was aligned

203   along a diagonal direction as shown in Fig. 5a. On the south side of the specimen, four LVDTs

204   were used: two in horizontal direction and two in vertical direction (Fig. 5b). The gage length for

205   horizontal and vertical LVDTs was 800 mm, and gage length for diagonal LVDTs was 1,130

206   mm.

207 The local strains on steel rebar and FRP sheets for each panel specimen were measured by a

208 total of 10 strain gauges. The position of strain gauges on steel rebar and FRP sheets are shown

209 in Fig. 6 and Fig. 7, respectively. It should be noted that the strain gauges on steel and FRP were

210 located at the same location.

211 A digital image correlation (DIC) system was used to obtain the displacement and deformation

212 field on the south side of the specimen. Through this DIC-based non-contact measurement

213 system, the crack spacing and crack width of the specimens were captured in real time. Load was

214 measured by the load cells installed on each hydraulic actuator.

215

216 **GENERAL BEHAVIOR OF TEST PANELS**

217 The specimens were subjected to pure shear loads in the *l-t* coordinates, as shown

218 previously in Fig. 4. The peak stresses and strains for all the test panels are listed in Table 2.

219 The subscript "m" indicates the load stresses at the peak shear stress and the subscript "0"

220 indicates the strains that are measured at the peak shear stress.

221 The shear stress, τ_{lt}, can be calculated in terms of the principle stress from Eq. (1) and the shear

222 strain, γ_{lt}, is determined form Eq. (2) as follows:

223 $\tau_{lt} = \dfrac{1}{2}(\sigma_1 - \sigma_2)$ (1)

224 $\gamma_{lt} = \varepsilon_1 - \varepsilon_2$ (2)

225 where σ_1 and σ_2 are the average horizontal tensile and vertical compressive stresses,

226 respectively; ε_1 and ε_2 are the average strains measured from LVDTs in horizontal and vertical

227 directions, respectively.

228 **Effect of FRP Stiffness on the Shear Behavior**

229   To study the shear behavior of FRP-strengthened RC members and to investigate the

230   effect of FRP stiffness, panels with same steel reinforcements in l and t directions, but different

231   FRP reinforcement ratios are tested. The application of FRP in the t-direction results in an

232   increase of effective reinforcement ratio in that direction. The effective reinforcement ratio is

233   defined as the contribution of transverse steel and FRP reinforcement ratio in the shear gain in t

234   direction. Therefore, a different behavior is expected to be observed. To compare the behavior of

235   panels, the shear stress-strain curves of panels series P4-FW, with the same steel reinforcement

236   ratio in l and t directions ($\rho_l = \rho_t = 0.76\%$) and different FRP reinforcement ratios (FRP

237   Stiffness) fully wrapped, are shown in Fig. 8. It can be observed that with the increase of FRP

238   stiffness, the shear strength of panels increases. The maximum shear strength of test panels P4-

239   025-FW, P4-040-FW, and P4-080-FW were 4.2 MPa, 5.6 MPa, and 6.3 MPa, respectively. With

240   the increase of FRP stiffness, the stiffness of strengthening system increases and the contribution

241   of FRP reinforcement to shear capacity will increase; therefore, the shear strength of panels

242   increases. The presence of FRP sheets along the transverse direction delays the yielding of steel

243   rebar in the t-direction. Therefore, the rebar in the longitudinal direction will yield sooner

244   compared to the rebar in the transverse direction. In other words, the rebar in l and t directions

245   will not yield at the same time as in panel REF-P4.

246   In order to compare the behavior of panels, the relationships between the shear stress and

247   average strain in longitudinal and transverse directions of panels series P4-FW are shown in Fig.

248   8. Panel REF-P4 is reinforced with equal amount of steel in l and t directions. Due to symmetry

249   of the loading and the reinforcements, the average strain in the l-direction, ε_l, equals the average

250   strain in the t-direction, ε_t. Therefore, the steel in both directions approximately yielded at the

251   same time. Also, the inclination of cracks in this case coincides with the direction

252   of principal compressive stress. Therefore, the interlocking action of aggregates

253   between concrete struts vanishes. As shown in Fig. 9, the measured strains in the two directions

254   for panel REF-P4 are very close to each other from the beginning of testing up to failure of the

255   panel. Panels in series P4-FW were reinforced with equal amount of steel in l and t directions

256   ($\rho_l = \rho_t = 0.76\%$). However, they were strengthened with different FRP reinforcement ratios

257   along the t-direction. Therefore, the presence of FRP sheets resulted in the increase of the

258   effective reinforcement ratio in transverse (t) direction and the steel in l-direction yielded sooner

259   than the steel in t-direction (Fig. 9). After steel yielded in both l and t directions, the average

260   strain in longitudinal direction ε_l increased rapidly compared to the average strain in transverse

261   direction ε_t. The FRP sheets aligned in the t-direction prevented the rapid increase of strain along

262   the transverse direction. It is observed from Fig. 9 that with the increase of FRP stiffness, the

263   difference in steel strains in l and t directions increases. For instance, in panel P4-025-FW, ε_l at

264   failure is 20% more than ε_t. With the increase of FRP reinforcement ratio this difference

265   increases. In panels P4-040-FW ($\rho_f = 0.87\%$) and P4-080-FW ($\rho_f = 1.74\%$), ε_l at failure is greater

266   than ε_t by 53% and 60%, respectively. With the increase of FRP reinforcement ratio (FRP

267   stiffness) in the transverse direction, the effective reinforcement ratio in the t-direction increases.

268   This will result in increase of deformation in the l-direction which is less reinforced.

269   **Effect of Wrapping Scheme on the Shear Behavior**

270   Wrapping scheme affects the confinement effect of the FRP sheets and the potential for

271   debonding. The effect of wrapping scheme on the shear stress-strain curves of the panels are

272   shown in Fig. 10 and Fig. 11. Test results of panels with the same steel and FRP reinforcement

273   ratios ($\rho_s = 0.76\%$, $\rho_f = 0.87\%$), but different wrapping schemes are shown in Fig. 10. The

274   behavior of panel P4-040-SB was similar to panel P4-040-FA up to failure. However, the shear

275 capacity of panel P4-040-FA was 22% greater than panel P4-040-SB. Panel P4-040-SB failed

276 due to premature debonding of FRP sheets. Panel P4-040-FW showed a different behavior

277 compared to the other two panels. The stiffness of the panel P4-040-FW after cracking was much

278 higher compared to P4-040-FA and P4-040-SB panels, which showed the same post cracking

279 behavior. This was due to a better bond between the FRP sheets and concrete substrate after

280 cracking of concrete in panel P4-040-FW, which resulted in the increase of the overall stiffness.

281 The shear capacity of panel P4-040-FW was 6% and 30% higher than panels P4-040-FA and P4-

282 040-SB, respectively. In Fig. 11, test results of panels with the same steel and FRP reinforcement

283 ratios ($\rho_s = 0.76\%$, $\rho_f = 0.43\%$), but different wrapping schemes are compared. Although it was

284 expected that the two panels show a similar behavior up to failure, the shear capacity of panel

285 P4-025-FA was 15% higher than panel P4-025-FW. This difference was due to a lower concrete

286 compressive strength, f_c', of panel P4-025-FW (45 MPa) compared to panel P4-025-FA (52

287 MPa). The contributions of steel and FRP on the overall shear capacity of the two members were

288 similar. However, the lower concrete compressive strength resulted in a lower contribution of

289 concrete on the overall shear capacity of panel P4-025-FW therefore, a lower overall shear

290 capacity was observed compared to panel P4-025-FA.

291 For design purposes, the strengthening scheme is selected based on factors such as the

292 accessibility of the member and the required amount of increase in shear capacity. The

293 recommended wrapping scheme is fully wrap for shear strengthening of the member whenever it

294 is possible. However, in most situations, a U-wrap with FRP anchor is the only economical and

295 practical economical and practical wrapping scheme.

296 **Effect of Transverse Steel Reinforcement on the Shear Behavior**

297   The panels were reinforced with two levels of transverse steel reinforcement ratios,

298    $\rho_t = 0.43\%$ and 0.76%. A low transverse reinforcement ratio (using No. 3 rebar) was chosen to

299   simulate a beam which is lightly reinforced, and a high transverse reinforcement was chosen to

300   simulate a beam which is heavily reinforced. The shear stress-strain curves of panels with the

301   same FRP reinforcement ratio and wrappings scheme, but different transverse reinforcement

302   ratios are compared in Figs. 12 and 13. The shear stress-strain curves of panels P3-040-FW and

303   P4-040-FW are compared in Fig. 12. The panels are reinforced with the same FRP reinforcement

304   ratio ($\rho_f = 0.87\%$) and the wrapping scheme is fully wrap. It can be observed that panel P4-040-

305   FW had 25% higher shear strength compared to panel P3-040-FW, due to a higher transverse

306   reinforcement ratio.

307   In Fig. 13, the shear stress-strain curves of panels P3-025-FW and P4-025-FW are compared.

308   The panels are reinforced with the same FRP reinforcement ratio ($\rho_f = 0.54\%$) and the wrapping

309   scheme is fully wrap. The two panels showed similar behavior in terms of maximum shear stress.

310   It was expected that panel P4-025-FW show higher shear strength compared to panel P3-025-

311   FW. Although, panel P4-025-FW had a lower concrete compressive strength ($f_c' = 45$ MPa)

312   compared to panel P3-025-FW ($f_c' = 51$ MPa), panel P3-025-FW reached its peak strength at a

313   lower shear stress and strain compared to panel P4-025-FW.

314   In Fig. 14, the strain of FRP sheets and transverse steel, measured using strain gauges, for panels

315   P4-040-FW and P3-040-FW are compared at same load levels. It is observed that both the

316   external FRP reinforcement and the transverse steel reinforcement did not contribute to the load-

317   carrying capacity in the initial stage of loading. This contribution initiated and became effective

318   after the first cracking occurred. In panel P4-040-FW it can be observed that before reaching the

319   tensile strength of concrete, the strains in FRP and steel were very small and less than the

320   maximum tensile strain of concrete. Once cracking occurred, strains on both steel and FRP

321   increased suddenly. Before yielding of the steel, FRP strain was higher than the steel strain at the

322   same load level. After steel yielded, the steel strain rapidly increased compared to FRP strain.

323   The same behavior was observed for panel P3-040-FW. In panel P3-040-FW immediately after

324   the steel yielded, since the transverse steel reinforcement ratio was low, the steel strain increased

325   rapidly and became higher than FRP strain at the same shear stress level. In panel P4-040-FW,

326   immediately after steel yielded, the transverse steel strain did not get bigger than the strain of

327   FRP. This was due to a larger steel reinforcement ratio compared to panel P3-040-FW, and due

328   to the different yield behavior of rebar Nos. 3 and 4 compared to each other. The strains in the

329   FRP and the transverse steel are different, even at the same locations, because the strain on the

330   fiber sheets increases drastically near the crack, due to the bond between the FRP and the

331   concrete substrate. Also, the crack widths are smaller at the rebar location and increase at the

332   surface. Addition of the FRP sheets delayed the contribution of transverse steel to the load

333   carrying capacity of the specimen. The results clearly show that the effect of externally bonded

334   FRP sheets preserves the integrity of internal transverse steel reinforcements. The effectiveness

335   of the contribution of FRP sheets to the shear gain highly depends on the amount of internal

336   shear steel reinforcement. However, the design guidelines have not yet considered the effect of

337   transverse steel reinforcement and the contribution of FRP on the overall shear response (V_f) in

338   their formulations.

339   **Failure Modes Associated with FRP-Strengthened RC Panels**

340   In RC members subjected to compression-tension biaxial stresses, various types of shear failure

341   occur; such as diagonal cracking, splitting, shear-compression failure, and web crushing[15].

342   These all involve cracking and crushing of concrete in a biaxial stress state. In FRP-strengthened

343   RC members, additional failure modes were observed. The two main failure modes related to the

344   FRP strengthening which were observed in test panels are FRP rupture and FRP debonding. In

345   the case of FRP rupture, the fibers reached their ultimate strain value and fracture at the point of

346   maximum stress. In the FRP debonding failure mode, the strain of FRP at ultimate stage were

347   considerably lower than the rupture strain. The failure mode of FRP rupture is similar to shear

348   tension failure in conventional RC beams where vertical flexural cracks originates from the

349   tension face. Widening of the diagonal crack eventually leads to failure involving tearing of the

350   FRP along a line corresponding to the diagonal shear crack in the concrete. Available

351   experimental data in literature shows that all of the test specimens with FRP sheets bonded on

352   sides only, and many bonded with U-wrap, failed by debonding of the FRP from the concrete

353   substrate.

354   The main failure modes associated to panel specimens are shown in Table 3. Fig. 15 shows the

355   main failure modes observed in panel specimens. In panels P3-FW and P4-FW series, which

356   were strengthened with fully wrap scheme, the main observed failure modes were FRP rupture

357   followed by crushing of concrete (Fig. 15a), except for panel P4-080-FW which failed by

358   concrete crushing prior to FRP failure (Fig. 15b). Concrete crushing occurred due to high

359   principal compressive stresses in the region between induced cracks. This failure mode is

360   normally associated with high amounts of transverse reinforcement but may also be critical in

361   beam members with thin webs. Panel P4-080-FW, which was strengthened with a higher FRP

362   reinforcement ratio compared to other panels (ρ_f = 1.74%), had a different failure mode. The

363   governing failure mode in this panel was concrete crushing. The increase in amount of FRP

364   reinforcement (increase in thickness of FRP sheets) resulted in decrease of active bond length,

365   that is the length which the majority of bond is maintained. Therefore, the effective strain in the

366   FRP sheets decreases and ultimately, FRP sheets did not reach their expected capacity up to their

367   tensile strength before rupture and the panel failed due to concrete crushing.

368   In panels P4-FA series, which were strengthened using U-wrap with FRP anchor wrapping

369   scheme, a mixed failure mode was observed. In panel P4-025-FA, anchorage failure was

370   observed on the south side of the panel while on the north side FRP rupture of FRP sheets was

371   seen (Fig. 15c). In panel, P4-040-FA, FRP anchors did not show any sign of failure and the

372   failure mode of the panel was governed by rupture of FRP sheets. This could be associated with

373   different bond between FRP and concrete substrate on both sides of the panel. On the south side

374   of the panel, the FRP anchors engaged in the shear resistance once the FRP sheets debonded

375   from the concrete surface and failed at their ultimate load carrying capacity.

376   Panel P4-040-SB, was strengthened with the side bond wrapping scheme. Once the concrete

377   cracked, local debonding of FRP sheets initiated from the concrete substrate and the panel

378   ultimately failed by debonding of all FRP sheets at a lower load level compared to other

379   strengthened panels (Fig. 15d). In this panel, the FRP was not able to utilize its full tensile

380   capacity and therefore, debonding of FRP sheets at lower strain levels occurred, which lowered

381   the efficiency of the strengthening system. In this mode of failure, once the FRP starts to peel

382   off, the beam will fail very quickly in a brittle process. The bond strength between FRP and

383   concrete thus plays the key role in this mode.

384   It should be noted that the strain distribution in the FRP along a shear crack is non-uniform

385   because the width of the critical shear crack changes from the lower end to the upper crack tip

386   [34]. This leads to a non-uniform strain distribution in the FRP because the strain anywhere in

387   the FRP intersected by the crack is closely related to the width of the crack at that location. Since

388   the FRP sheets are linear elastic material up to their rupture, the stress in the FRP is also non-

389　uniform along the shear crack. Combined with the brittle behavior of FRP, this means that at

390　any instant in the failure process, only the most highly stressed part of the FRP is at its full

391　tensile capacity.

392　　　In practice, for design of FRP strengthened RC members, the primary failure modes are

393　selected for each element. Each failure mode is classified in terms of the type of failure it

394　represents and the seriousness of damage it causes [35]. A primary failure mode should be

395　considered followed by other failure modes and their degree of undesirability. For instance, in an

396　RC beam strengthened with FRP, the most desirable failure mode is flexural concrete crushing

397　and the least desirable is debonding. For shear strengthening, the failure modes and bond of

398　FRP to concrete substrate remain the focus of many research work. There are several verities in

399　failure modes in FRP strengthened systems which can govern the strength [1]. While most of the

400　failure modes have been identified by researchers, more accurate methods are still required.

401　Throughout the design procedures, significant limitations on the strain and stress level achieved

402　in the FRP material are imposed to conservatively account for debonding failure modes. More

403　thorough design guidelines should be incorporated in codes for predicting debonding and other

404　failure modes.

405
406　**CRACK CHARACTERISTICS**

407　The evolution of strains and deformations on FRP and concrete have been measured with a DIC

408　system and its tracking method. This method has been widely used for measurements in RC and

409　masonry members [36-38]. In order to study the crack characteristics on panel specimens, the

410　DIC system was used on the south side of the specimen. The DIC system will generate contour

411   plots of the axial and lateral surface deformations of the panels, which will help determine the

412   exact pattern around and in between the FRP sheets [19].

413   The crack characteristics including crack width, spacing, and amount were measured by the DIC

414   system and are presented in the following sections. In Fig. 16, the strain field in the direction of

415   applied horizontal load ε_x of a specimen at a specific load level is shown using color gradient.

416   The cracks are identified at locations with sudden increase in strain. The crack widths are

417   measured by assigning two points near the cracks and continuously measuring their distances. It

418   should be mentioned that due to accessibility issue, the DIC system was not used for specimen

419   P4-025-FW, P4-040-FA, and P4-040-SB. The integrity of a structure is affected by the crack

420   characteristics and therefore careful considerations should be made [39].

421   **Crack Spacing**

422   The stabilized cracking phase is reached when the crack spacing between two existing

423   cracks are too small for a new crack to develop in between. The crack spacing was determined at

424   the last phase of the testing, since it is closest to the stabilized cracking stage. In Table 4,

425   experimental measurements of the average crack spacing, S_{rm}, maximum crack spacing, $S_{r,max}$,

426   and minimum crack spacing, $S_{r,min}$, in panel specimens subjected to shear are presented. The

427   experimental average crack spacing is defined by the measurement of the spacing between the

428   adjacent cracks on the panel at different heights and averaging for the entire specimen at the

429   stabilized cracking stage. The maximum and minimum crack spacing is defined based on the

430   maximum and minimum measured crack spacing at the stabilized cracking stage throughout the

431   specimen, respectively. In Fig. 17, ratios of maximum and minimum to average crack spacing

432   versus average crack spacing in shear tests of panel specimens are presented. The mean value of

433   the ratio $S_{r,max}/S_{rm}$ and $S_{r,min}/S_{rm}$ are shown with horizontal dashed lines. In EC2-04 [40] a value

434   of 1.7 is assumed for the ratio of the maximum to average crack spacing for RC structures; which

435   is observed to be higher compared to the experimental value of $S_{r,max}/S_{rm}$ that equals 1.47 for

436   FRP-strengthened RC panels.

437   **Crack Width**

438   Using the DIC system the crack widths were measured continuously during the test. It was

439   observed that in FRP-strengthened RC members; average crack widths were generally smaller

440   than for un-strengthened members at the same shear strain level (Fig. 18), due to the additional

441   bond action developing at the FRP-concrete interface. Although, the number of cracks did not

442   increase significantly in strengthened members as shown in Table 4., the crack widths decreased

443   compared to RC panels. The thicker FRP (1.0 mm) provided better crack control compared to the

444   thinner FRP (0.6 mm). Similar results were observed for P4-FW and P4-FA series. As shown in

445   Fig. 19, in panels strengthened with FRP, average crack widths were generally smaller than un-

446   strengthened RC panels at the same shear strain level. For panels P4-FW series, with the increase

447   of FRP reinforcement ratio, the crack widths did not change significantly at lower shear strains.

448   In general. specimens strengthened with FRP exhibited a greater tension stiffening effect

449   compared to RC specimens. The contribution of the concrete in shear affects the overall stiffness

450   of the FRP strengthened RC members after cracking. Therefore, the crack spacing and crack

451   width are affected at service load level. Wrapping scheme and FRP reinforcement ratio affect the

452   bond behavior of steel-concrete and, FRP-concrete interface in FRP strengthened RC members.

453   This will result in a different crack pattern in such members compared to RC members.

454   MATHEMATICAL MODELING OF SMEARED STRESS-STRAIN CURVES OF FRP

455   STRENGTHENED RC IN COMPRESSION

456　　The softening coefficient is the most important parameter affecting the smeared

457　　stress-strain relationships of concrete in compression. Several researchers have

458　　investigated the softening coefficient in RC members and determined that the most

459　　effective parameters are: concrete compressive strength, f_c', the uniaxial tensile

460　　strain, $\bar{\varepsilon}_1$, and the deviation angle, β [13,14]. In case of FRP strengthened RC

461　　members, the FRP sheets also have significant effect on the softening of concrete

462　　[16]. The smeared constitutive relationship of concrete compressive stress, σ_2^c,

463　　versus the uniaxial compressive strain, $\bar{\varepsilon}_2$, in the Softened Membrane Model, shown

464　　in Fig. 20, is given as:

465　　$$\sigma_2^c = \zeta f_c' \left[2\left(\frac{\bar{\varepsilon}_2}{\zeta \varepsilon_0} \right) - \left(\frac{\bar{\varepsilon}_2}{\zeta \varepsilon_0} \right)^2 \right] \qquad \text{when } \frac{\bar{\varepsilon}_2}{\zeta \varepsilon_0} \leq 1 \text{ and} \tag{2}$$

466　　$$\sigma_2^c = \zeta f_c' \left[1 - \left(\frac{\left(\bar{\varepsilon}_2 / \zeta \varepsilon_0 \right) - 1}{\left(4 / \zeta \right) - 1} \right)^2 \right] \qquad \text{when } \frac{\bar{\varepsilon}_2}{\zeta \varepsilon_0} > 1 \tag{3}$$

467　　The softening coefficient in Eq. 2 and 3 is expressed as the product of the function of concrete

468　　compressive strength, f_c', uniaxial tensile strain, $\bar{\varepsilon}_1$, and deviation angle, β, as

469

470　　$\zeta = f(f_c')f(\bar{\varepsilon}_1)f(\beta)$, where $\tag{4}$

471　　$f(f_c') = \dfrac{5.8}{\sqrt{f_c'}} \leq 0.9$ $\tag{5}$

472　　$f(\bar{\varepsilon}_1) = \dfrac{1}{\sqrt{1 + 400\bar{\varepsilon}_1}}$, $\tag{6}$

473　　$f(\beta) = 1 - \dfrac{|\beta|}{24^o}$ $\tag{7}$

474　　Previous researches showed that in FRP strengthened RC members, FRP reinforcement has

475   significant effect on the softening coefficient [9 ,16]. Therefore, in FRP strengthened members

476   the softening coefficient is expressed as

477      $$\zeta_{FRP} = f(f'_c)f(\bar{\varepsilon}_1)f(\beta)f(FRP)$$ (8)

478   where, the first three terms on the right-hand side of Eq. (8) are the same as the

479   softening coefficient for RC, Eq`ns. (5) to (7), proposed by other researchers at

480   University of Houston [14, 18,41]. The fourth term is proposed by Yang [9] as

481      $$f(FRP) = 1 + 0.0076\sqrt{\rho_f E_f}$$ (9)

482   In the proposed equation, $\rho_f E_f$ were adopted to account for the area of the

483   concrete. It should be noticed that the proposed equation converges to the result of

484   RC when $\rho_f E_f$ equals to zero, in which case f (FRP) equals to 1 and the expression

485   will be the same as for RC.

486   To express the smeared stress-strain curves of the concrete in compression in

487   FRP strengthened RC members, the same parabolic equation, Eq. (2) and (3), is

488   used. The softening coefficient is derived from Eq. (8). The experimental results of

489   FRP strengthened RC panels subjected to shear will be used to validate the function

490   of deviation angle, β, in the softening equation of RC members for FRP

491   strengthened RC members.

492   The angle β is the deviation angle between r-d coordinate and 1-2 coordinate,

493   equal to α_r-α_1 (Fig. 21). β is a function of the strain state, and can be expressed in

494   terms of the three strains, ε_1, ε_2, and γ_{12} using the compatibility equations as

495      $$\beta = \frac{1}{2}\tan^{-1}\left[\frac{\gamma_{12}}{\varepsilon_1 - \varepsilon_2}\right]$$ (10)

496

497   The deviation angle, β, is equal to zero if the element is reinforced with the

498 same amounts of steel bars in l and t directions and subjected to pure shear loading,

499 e.g., REF-P4. The values of β and $f(\beta)$ from FRP strengthened RC panel tests are

500 listed in Table 5. The concrete compressive strength, f_c', and the uniaxial tensile

501 strain, $\bar{\varepsilon}_1$, of the concrete in the 1-direcrion at the peak point of the shear stress-

502 strain curve for each panel are listed in Table 5. The values of $f(f_c')$, $f(\bar{\varepsilon}_1)$ and

503 $f(FRP)$ are calculated using Eqns. (5, 6, and 9), respectively. Dividing the

504 experimental value of the softening coefficient, ζ_{exp}, by $f(f_c')$, $f(\bar{\varepsilon}_1)$, and $f(FRP)$ the

505 experimental $f(\beta)$ for each panel is obtained and listed in Table 5. The value of β

506 for each panel is calculated using Eq. (10).

507   According to the data in Table 5, the $f(\beta)_{exp}$ versus β relationships for the

508 FRP strengthened RC panels is plotted in Fig. 20 along with the data for the

509 reinforced concrete panel tests [18, 41]. Also, the straight line defined by Eq. (7) is

510 plotted in Fig. 20.

511 The $f(\beta)_{exp}$ versus β relationships for FRP strengthened RC panels show a different

512 trend than that for RC panels. Therefore, Eq. (7) should be modified before it can

513 be applied to FRP strengthened RC members. Similar to RC members, the

514 relationship between β and $f(\beta)$ is approximately linear. A regression analysis of

515 the FRP strengthened RC data is performed to develop the new function of the

516 deviation angle, β, in the softening coefficient of FRP strengthened RC members as

517 $$f_{FRP}(\beta) = \left(1 - \frac{|\beta|}{16^o}\right)$$ (11)

518 The effect of deviation angle, β, on the softening coefficient in FRP strengthened RC members is

519 more complicated than that in RC members. The presence of FRP along the transversal direction

520 increases the stiffness in that direction and therefore, increases the difference in the stiffness in

521 the l and t directions. Thus, the deviation angle increases followed by a decrease in the softening

522 coefficient. The new function of the deviation angle, $f_{FRP}(\beta)$, has been used for the softening

523 equation of the new softened membrane model for FRP strengthened RC members presented

524 elsewhere [42].

525
526 **CONCLUSIONS**

527 In order to evaluate the shear behavior of FRP-strengthened RC members and investigate

528 the main factors which influence its behavior, panel testing was carried out. Other testing

529 techniques such as testing beam with various a/d ratios cannot predict the true pure shear

530 behavior due to the presence of flexural and other non-shear related effects that cannot be filtered

531 out. For this purpose, full-scale tests on 8 FRP-strengthened RC panels and 2 RC panels were

532 conducted. It should be noted that in this research the initial stresses existing in members prior to

533 strengthening have been considered. The effects of different parameters on the true shear

534 behavior of FRP-strengthened RC members were investigated. The following conclusions can be

535 made:

536 1) It was found that the application of FRP sheets enhanced the overall shear behavior of RC

537 panels. However, ductility of the specimens was reduced due to the failure modes associated

538 with the strengthening system such as FRP rupture and FRP debonding.

539   2) The presence of FRP sheets resulted in the increase of the effective reinforcement ratio in

540   transverse direction, and the steel in the l-direction yielded sooner than the steel in the t-

541   direction. After the steel yielded in both l and t directions, the strain in the longitudinal direction,

542   ε_l, increased rapidly compared to the strain in the transverse direction, ε_t. The FRP sheets aligned

543   in the t-direction prevented the rapid increase of strain along the transverse direction. Also, with

544   the increase of FRP reinforcement ratio, the difference in steel strains in l and t directions

545   increased.

546
547   3) In this research, many failure modes of FRP strengthened RC members have been identified.

548   While some of these failure modes are similar to those of RC members, others are unique to FRP

549   strengthened members. The transfer of stresses from concrete to FRP sheets is a critical

550   parameter in FRP strengthening since it is likely to cause undesirable premature and brittle

551   failures. The two main failure modes observed in the tests were rupture of FRP sheets at the

552   ultimate strain following the yielding of internal steel reinforcement and debonding of FRP

553   sheets in a brittle manner with a thin layer of concrete residue attached to the delaminated FRP

554   sheet. It was observed that wrapping schemes played a critical role in determining the failure

555   mode of the strengthened member. While all specimen with side bond wrapping scheme failed

556   by premature FRP debonding, most specimens with U-wrap plus FRP anchor and fully wrap

557   failed by concrete crushing followed by rupture of FRP.

558   4) It was observed that the magnitude of increased shear capacity associated with the application

559   of FRP sheets depend not only upon the amount of FRP reinforcement that is being used, but

560   also on the amount of internal shear reinforcement. The increase in transverse steel reinforcement

561   resulted in a significant decrease in the shear gain due to FRP strengthening. There exists a high

562   interaction between the components of the strengthening system, specifically steel and FRP

563   reinforcement, when subjected to shear. The strains in the FRP sheets and the internal transverse

564   steel reinforcement were observed to be different at the same locations in the test region. This

565   was due to the strain on the fiber sheets increasing drastically near the cracks, due to the bond

566   between the FRP and the concrete substrate. With increase in the internal shear reinforcement

567   ratio, the crack pattern becomes relevantly more distributed along the member and therefore, the

568   available effective bond length decreases. This ultimately leads to decrease in the bond force and

569   decrease in the effectiveness of the FRP strengthening scheme. It should be noted that the

570   external FRP reinforcement does not prevent the internal transverse steel reinforcement from

571   yielding rather delays it.

572   5) Test results showed that applying FRP reinforcement significantly changed the crack width

573   and spacing of the RC member. The contribution of the concrete in shear affects the overall

574   stiffness of the FRP strengthened RC members after cracking. Therefore, the crack spacing, and

575   crack width are affected at service load level. Different wrapping schemes and external FRP

576   reinforcement ratio affects the bond behavior of steel-concrete and also FRP-concrete interface

577   in FRP strengthened members. This will result in different crack patter in in such members

578   compared to RC members. Average crack widths were generally smaller than for un-

579   strengthened RC members at the same smeared strain level due to the additional bond action

580   developing at the FRP-concrete interface which further reduced the crack spacing.

581   6) The softening coefficient is the most important parameter affecting the smeared stress-strain

582   relationships of concrete in compression. Previous research studies showed that in addition to

583   effective parameters in the softening coefficient of RC members, FRP sheets also have

584   significant effect on the softening of concrete in FRP strengthened RC members. In this paper, a

585 new softening coefficient for FRP strengthened reinforced concrete in compression is proposed

586 based on panel tests. The new softening coefficient includes the modified deviation angle factor

587 in terms of the deviation angle β. The presence of FRP along the transversal direction increases

588 the stiffness in that direction and therefore, increases the difference in the stiffness in the l and t

589 directions. Thus, the deviation angle increases followed by a decrease in the softening

590 coefficient. The new function of the deviation angle was implemented in the softening equation

591 of the new softened membrane model for FRP strengthened RC members presented elsewhere.

592

597 **REFERENCES**

598 [1] ACI Committee 440. Guide for the design and construction of externally bonded FRP

599 systems for strengthening concrete structures. ACI 440.2R-08. Farmington Hills (MI):

600 American Concrete Institute; 2008.

601 [2] A. Khalifa, A. Nanni. Improving shear capacity of existing RC T-section beams using CFRP

602 composites. Cem. Conc. Compos., 22(2000) 165-174.

603 [3] H. Baghi, JA. Barros, F. Menkulasi. Shear strengthening of reinforced concrete beams with

604 Hybrid Composite Plates (HCP) technique: experimental research and analytical model. Eng.

605 Struct. 125(2016) 504–20.

606 [4] B. B. Adhikary, H. Mutsuyoshi, M. Ashraf. Shear strengthening of reinforced concrete

607 beams using fiber-reinforced polymer sheets with bonded anchorage. *ACI Struc. J.* 101(2004)

608   660-668.

609   [5] AASHTO. AASHTO LRFD Bridge design specifications. Washington, DC. 2008.

610   [6] A. Belarbi,, S.W. Bae, A. Ayoub, D. Kuchma, A. Mirmiran, A. Okeil. Design of FRP

611   systems for strengthening concrete girders in shear. *NCHRP Rep. No. 678* Washinton D.C.

612   2011.

613   [7] M.A. Colalillo. Behavior of shear-critical reinforced concrete beams retrofitted with

614   externally applied fibre-reinforced polymers (Doctoral dissertation). Department of Civil

615   Engineering, University of Toronto, Toronto, Canada. 2012.

616   [8] A. Mofidi, O. Chaallal. Effect of steel stirrups on shear resistance gain due to externally

617   bonded fiber-reinforced polymer strips and sheets. ACI Struc. J. 111(2014) 353–361.

618   [9] G.Yang, M. Zomorodian, A. Belarbi, A. Ayoub A. Uniaxial Tensile Stress-Strain

619   Relationships of RC Elements Strengthened with FRP Sheets. J. Compos. Constr., 2015.

620   10.1061/(ASCE)CC.1943-5614.0000639, 04015075.

621   [10] H. Baghi, J.A. Barros. Shear strengthening of reinforced concrete T-beams with hybrid

622   composite plate. J. Compos. Constr., 20.6 (2016): 04016036.

623   [11] G. Monti, M.A. Liotta. Tests and design equations for FRP-strengthening in shear.

624   *Construction and Building Materials*, 21(2007) 799-809.

625   [12] V. Colotti, R.N. Swamy. Unified analytical approach for determining shear capacity of RC

626   beams strengthened with FRP. Eng. Struct. 33(2011) 827-842.

627   [13] T.T.C. Hsu, R.R.H. Zhu. Softened Membrane Model for reinforced concrete elements in

628   shear Struc. J. ACI. 99(2002) 460–469.

629   [14] A. Belarbi, T.T.C. Hsu. Constitutive laws of concrete in tension and reinforcing bars

630   stiffened by concrete. ACI Struc. J. 91(1994) 465-474.

631 [15] T.T.C. Hsu, Y.L. Mo. Unified theory of concrete structures. West Sussex, UK: John Wiley

632   and Sons Ltd. 2010.

633 [16] G. Yang, M. Zomorodian, A. Belarbi. Material Laws of FRP-Strengthened RC Element in

634   Biaxial Tension–Compression. *J. Compos. Constr.* 2017. 10.1061/(ASCE)CC.1943-5614.

635   20170000804.

636 [17] T.T.C. Hsu, L.X. Zhang, T. Gomez. A Servo-Control System for Universal Panel Tester. J.

637   Test. Eval., 23 (1995) 424–430.

638 [18] Pang, X. B., Hsu, T. T. C. (1996). Fixed-Angle Softened-Truss Model for reinforced

639   concrete. ACI Struct. J., l, 93(2), 197-207 [19] M. Zomorodian, G.Yang, A. Belarbi, A.S.

640   Ayoub. Cracking behavior and crack width predictions of FRP-strengthened RC members

641   under tension. *Eng. Struct.,* 125(2016) 313-324.

642 [20] A. Bousselham, O. Chaallal. Shear strengthening reinforced concrete beams with fiber-

643   reinforced polymer: assessment of influencing parameters and required research. *ACI Struc.*

644   *J.* 101(2004) 219–227.

645 [21] A. Bousselham, O. Chaallal. Effect of transverse steel and shear span on the performance of

646   RC beams strengthened in shear with CFRP. *Compos. Part B: Eng.*, 37(2006) 37–46.

647 [22] CAN/CSA S806-12. *Design and construction of building structures components with Fiber-*

648   *Reinforced Polymers.* Rexdale, Ontario, Canada. 2012.

649 [23] FIB (International Federation for Structural Concrete). FRP as externally bonded

650   reinforcement of R.C. structures: basis of design and safety concept. *Fib Bulletin 14*,

651   Lausanne, Switzerland. 2001.

652 [24] Triantafillou, T. C. (1998). "Shear strengthening of reinforced concrete beams using epoxy-

653   bonded FRP composites." *ACI Struc. J.*, *95*(2), 107–115.

654 [25] N. Eshwar, A. Nanni, T. Ibell. CFRP strengthening of concrete bridges with curved soffits.

655 *Proc., Int. Conf. on Structural Faults and Repairs*, Montreal, Quebec. 2003.

656 [26] G. Özdemir. *Mechanical properties of CFRP anchorage* (Master's Thesis). Department of

657 Civil Engineering, Middle East Technical University, Turkey. 2005.

658 [27] S.L. Orton. *Development of a CFRP system to provide continuity in existing reinforced*

659 *concrete buildings vulnerable to progressive collapse* (Doctoral dissertation). Department

660 of Civil, Architectural, & Environmental Engineering, University of Austin-Texas, Austin,

661 TX. 2007.

662 [28] Y. Kim, K. Quinn, J. Garcia,W. Sun, W. Ghannoum, J. Jirsa. *Shear strengthening of*

663 *reinforced and prestressed concrete beams using carbon fiber reinforced polymer (CFRP)*

664 *sheets and anchors (Technical Rep. 0-6306-1).* Austin, TX. 2012.

665 [29] K. Kobayashi,S. Fujii,Y. Yabe, H. Tsukagoshi, T. Sugiyama. Advanced wrapping system

666 with CF anchor-stress transfer mechanism of CF anchor. *Proc., of the 5th Int. Symp. on*

667 *FRP Reinf. for Conc. Struc. (FRPRCS-5)*. Cambridge. UK. 2001.

668 [30] E. Grande, M. Imbimbo, A. Rasulo. Effect of transverse steel on the response of RC beams

669 strengthened in shear by FRP: experimental study. *J. Compos. Constr.*, *13*(2009) 405-414.

670 [31] ASTM. Standard test method for compressive strength of cylindrical concrete specimens.

671 ASTM C39, West Conshohocken, PA. 2014.

672 [32] ASTM. Standard test method for tensile properties of polymer matrix composite materials.

673 ASTM D3039, West Conshohocken, PA. 2014.

674 [33] ASTM. Standard test method for pull-off strength for FRP bonded to concrete substrate.

675 ASTM D7522, West Conshohocken, PA. 2014.

676 [34] G. Chen, J. Teng, J. Chen. Shear strength model for FRP-strengthened RC beams with

677   adverse FRP-steel interaction. *J. Compos. Constr.* 17(2013) 50-66.

678   [35] K. Neocleous, K.Pilakoutas, P. Waldron. Structural reliability for fibre reinforced polymer

679   reinforced concrete structures. *Proc. of the 4th Int. Symp. on Fibre Reinf. Polymers for*

680   *Reinf. Conc. Struc.* (FRPRCS-4). Baltimore. Maryland. 65-74. 1999.

681   [36] M.M.R. Mousavi, M.D. Champiri, M.S. Joshaghani, S. Sajjadi. A kinematic measurement

682   for ductile and brittle failure of materials using digital image correlation. *AIMS Mat. Sci.*

683   3(2016) 1759-1772.

684   [37] S. Beizaee,K.J. Willam, G. Xotta,R. Mousavi. Error analysis of displacement gradients via

685   finite element approximation of digital image correlation system. *Proc., Of the 9th Int. Conf.*

686   *on Frac. Mech. of Conc. and Conc. Struc*. (FraMCoS-9), Berkeley, CA. 2016.

687   [38] M.D. Champiri, S.H. Mousavizadegan, F. Moodi. A decision support system for diagnosis

688   of distress cause and repair in marine concrete structures. *Comput. Concr.,* 9(2012) 99–118.

689   [39] M.D. Champiri, S.H. Mousavizadegan, F. Moodi. A fuzzy classification system for

690   evaluating the health condition of marine concrete structures. *J. Adv. Concr. Technol.*,

691   10(2012) 95–109.

692   [40] Eurocode-2. *Eurocode 2: Design of Concrete Structures-Part 1: General Rules & Rules for*

693   *Buildings*. Brussels, Belgium. 2004.

694   [41] Zhang, L. X., Hsu, T. T. C. (1998). Behavior and analysis of 100-MPa concrete membrane

695   elements. J. Struct. Eng., 124(1), 24-34.

696   [42] M. Zomorodian, A. Belarbi, A. Ayoub (2017). Finite element model for predicting the shear

697   behavior of FRP-strengthened RC members. Eng. Struct., 153(2017) 239-253.

698   **Figure Captions**

699   **Fig. 1.** Dimensions of test panels

31

a) FRP Layout · b) Rebar Layout
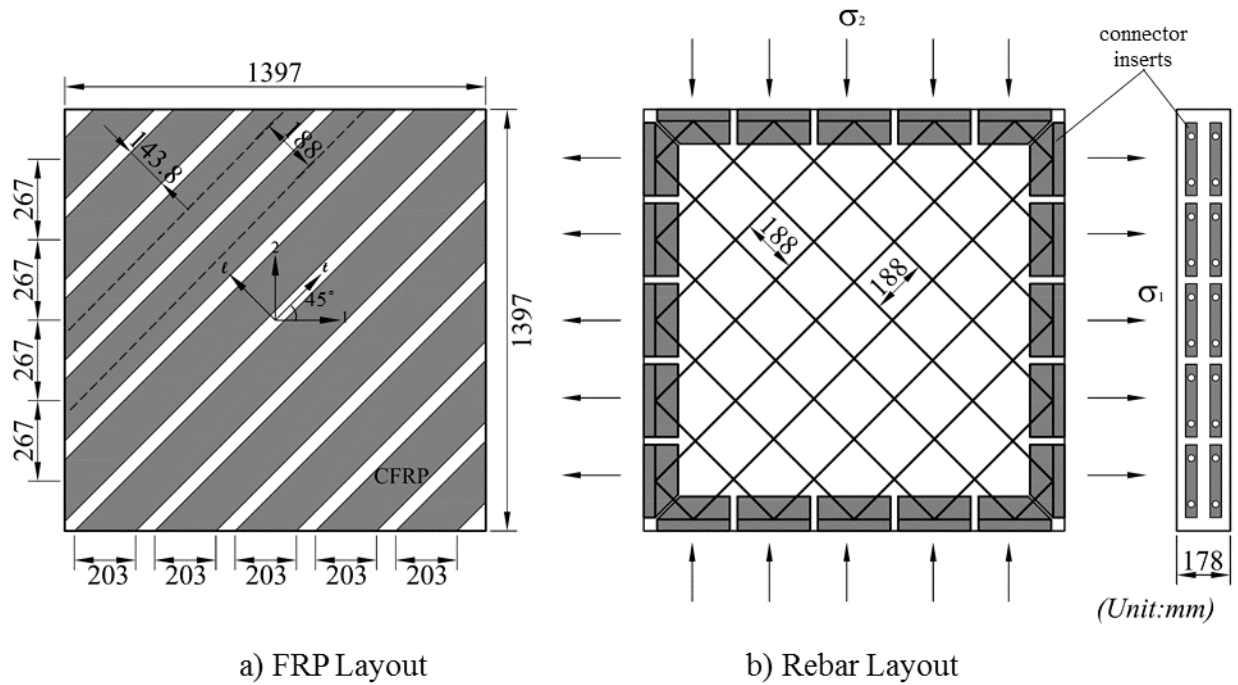
Fig. 1. Dimensions of test panels

a) FRP Layout · b) Fully Wrap · c) Side Bond

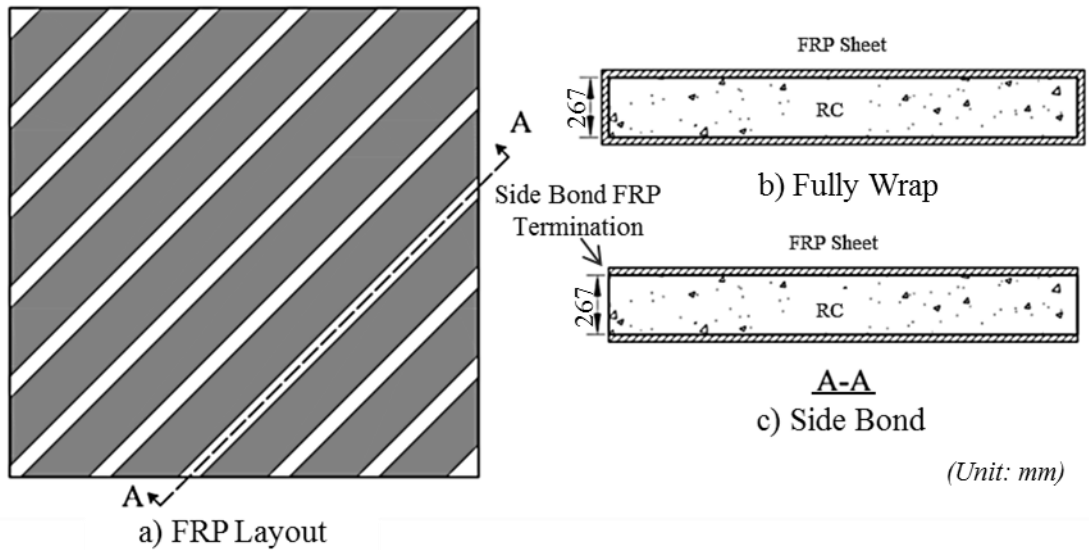**Fig. 2.** Layout and wrapping method of FRP sheets, a) FRP layout, b) Fully wrap, and c) Side bond wrapping scheme cross sections

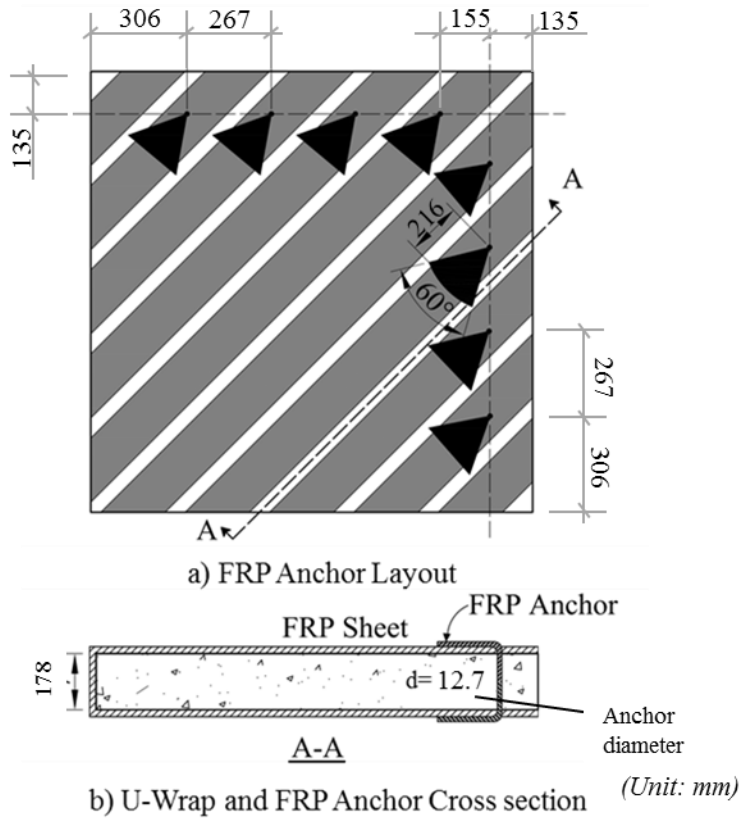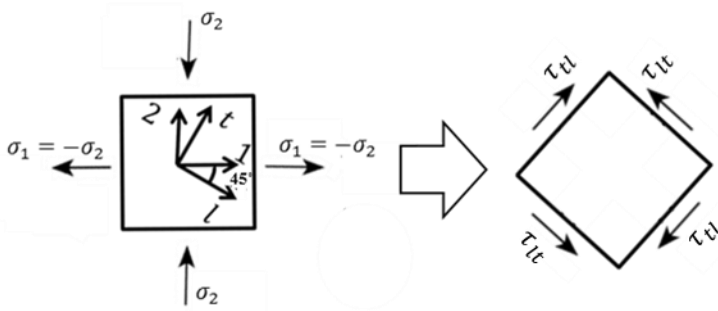a) FRP Anchor Layout

b) U-Wrap and FRP Anchor Cross section *(Unit: mm)*

Fig. 3. U-Wrap with FRP anchor details

Fig. 4. Proportional loading of panel in 1-2 directions

a) North Side   b) South Side
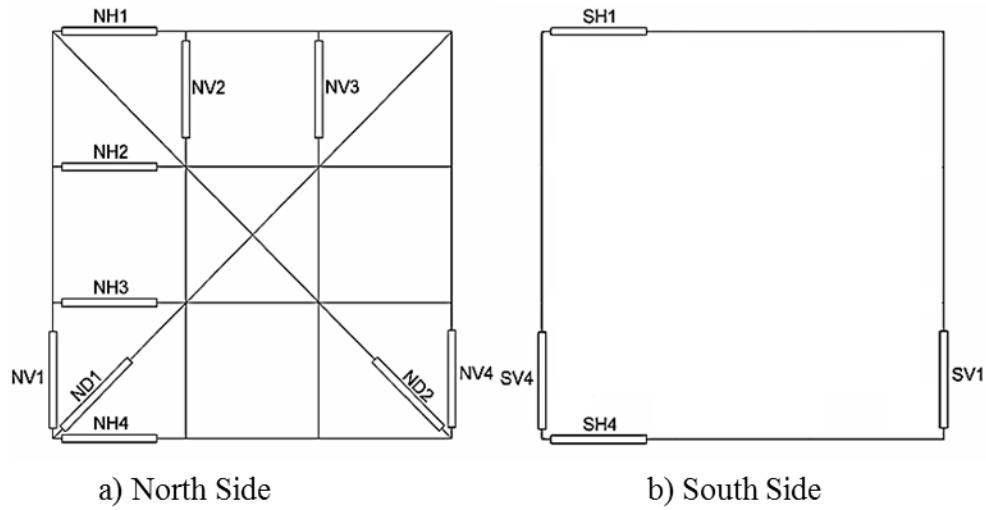
Fig. 5. LVDT arrangement for the panel specimens

_____ Transversal Rebar
_ _ _ _ Longitudinal Rebar

(Unit: mm)

a) North Side   b) South Side
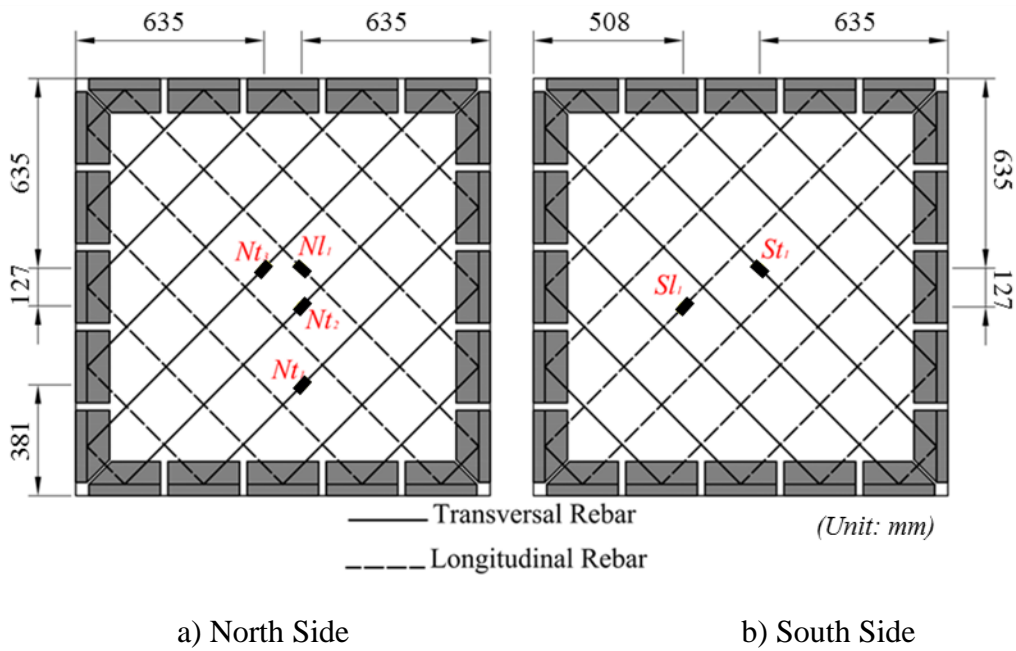
Fig. 6. Strain gauge layout on steel rebar of panel specimens

35

a) North Side   b) South Side
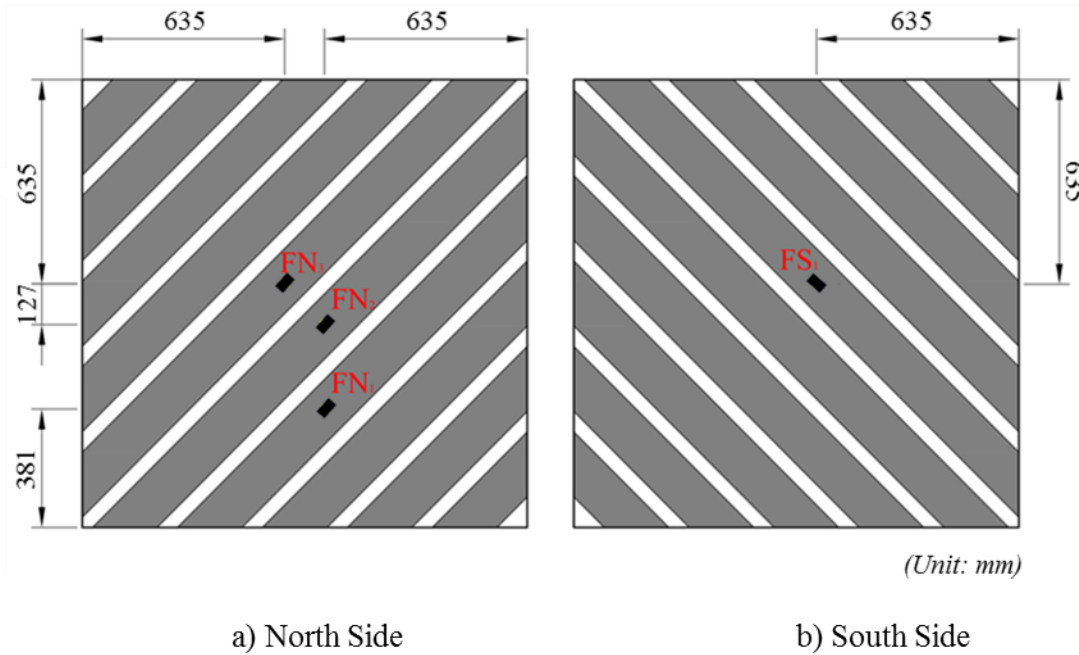
Fig. 7. Strain gauge layout on FRP sheets of panel specimens
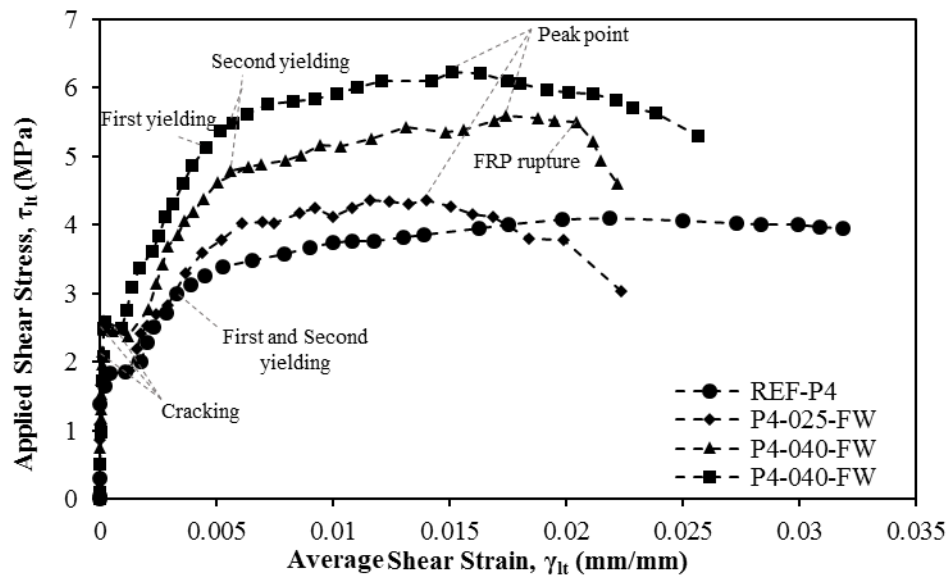
Fig. 8. Effect of FRP stiffness on shear stress-shear strain curves of panels P4-FW series
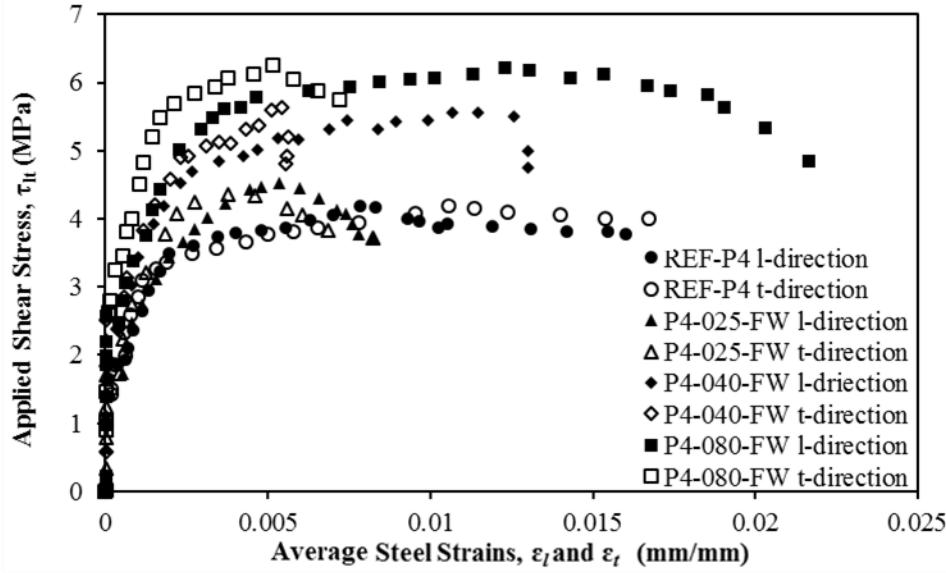
Fig. 9. Effect of FRP stiffness on $\tau_{lt} - \varepsilon_l$ and $\tau_{lt} - \varepsilon_t$ relationships of panels P4-FW series
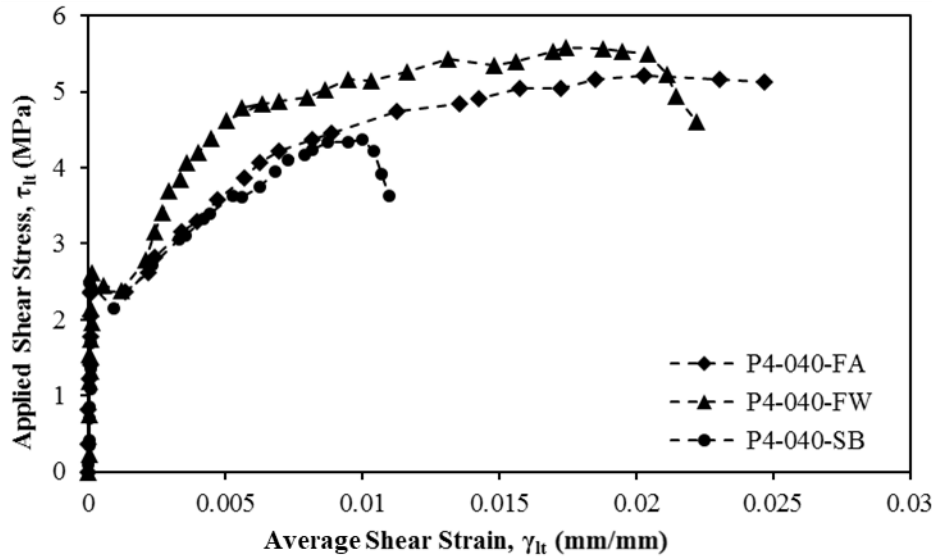
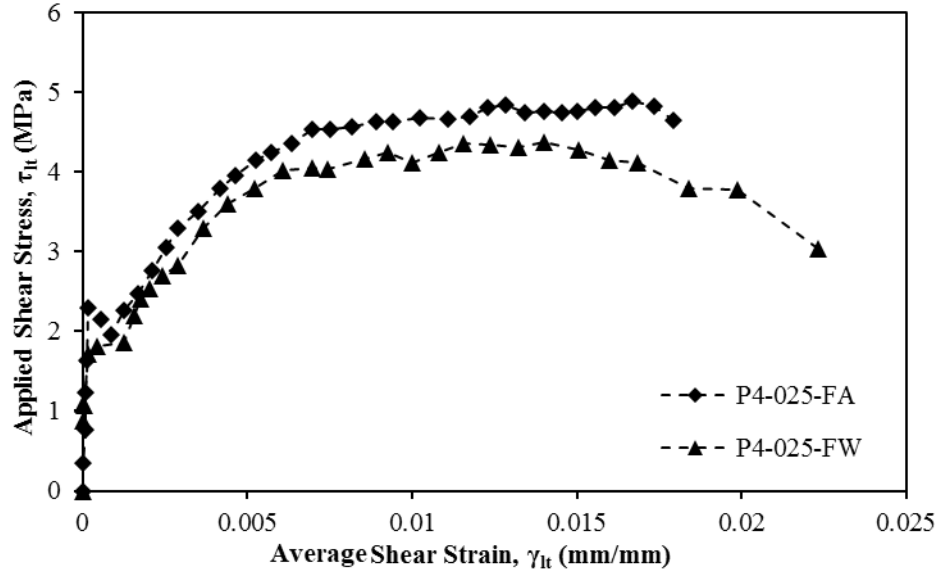**Fig. 10.** Shear stress-strain curves for specimens with different wrapping schemes (panels P4-040 series)

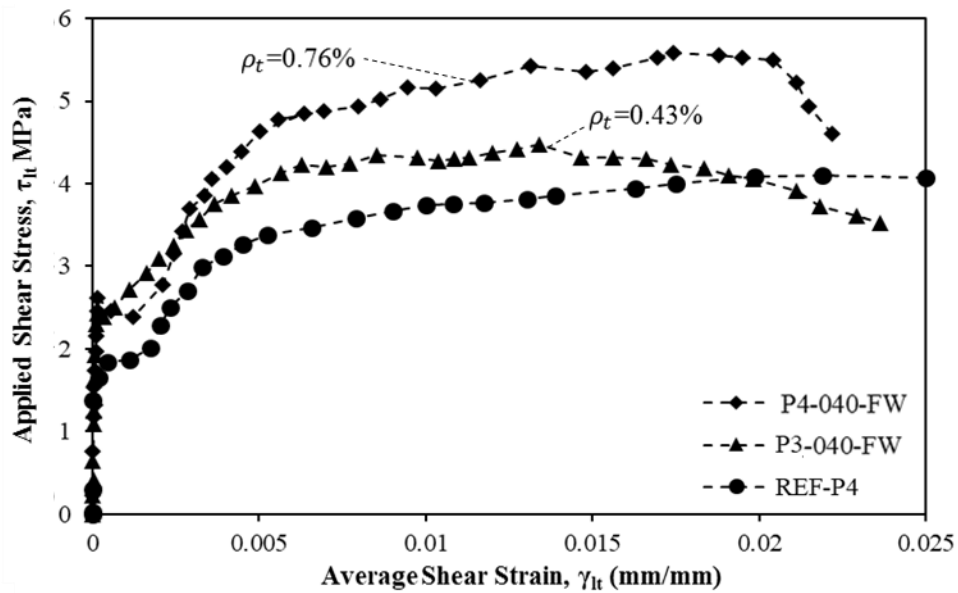**Fig. 11.** Shear stress-strain comparison of wrapping scheme in panels P4-025 series

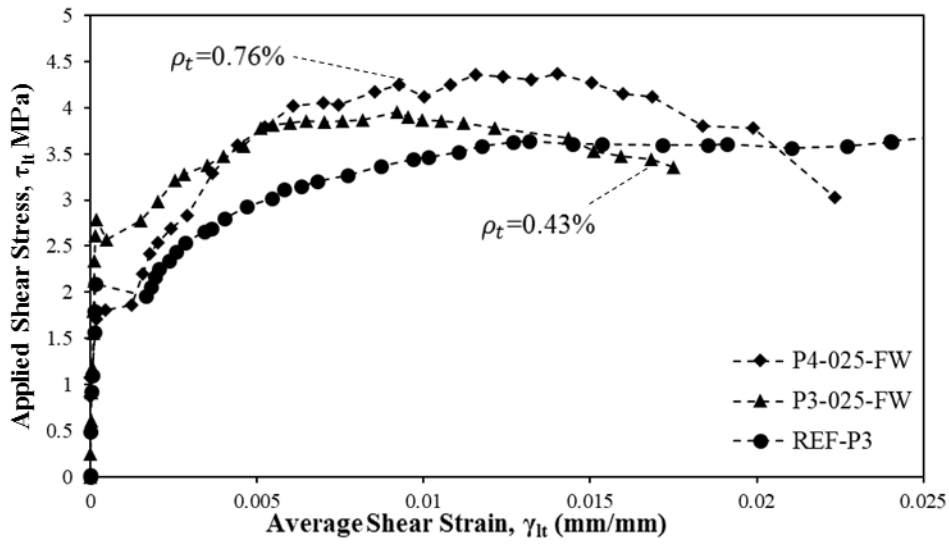**Fig. 12.** Shear stress-strain comparison of transverse steel reinforcement in panels 040-FW series

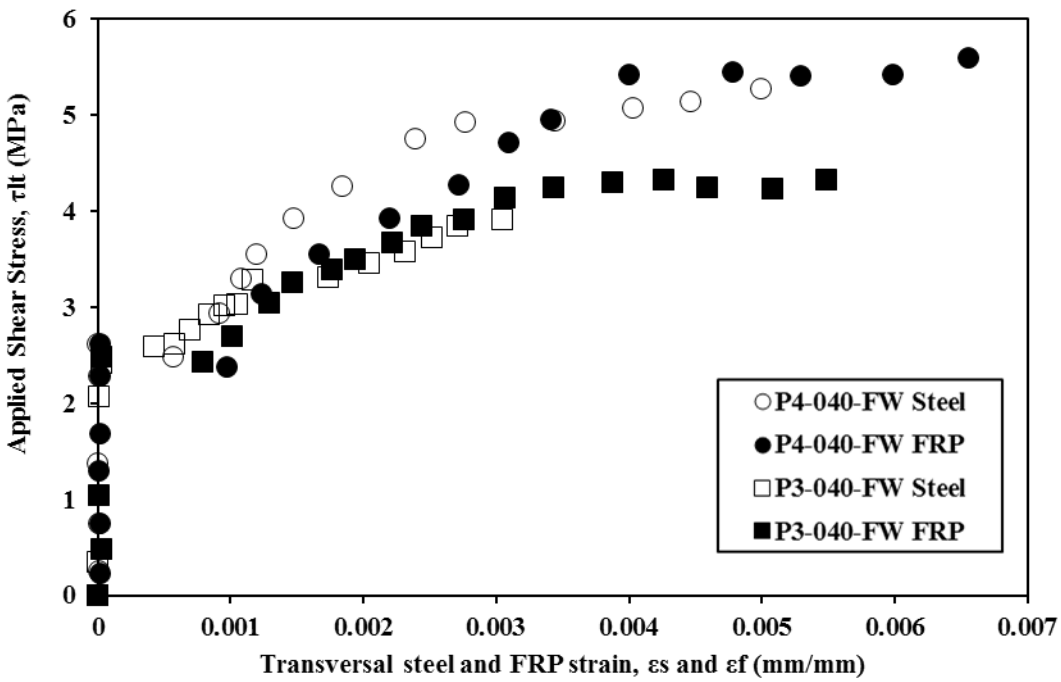**Fig.13.** Shear stress-strain comparison of transverse steel reinforcement in panels 025-FW series

Fig. 14. Comparison of transverse steel strain and FRP of panels P4-040-FW and P3-040-FW
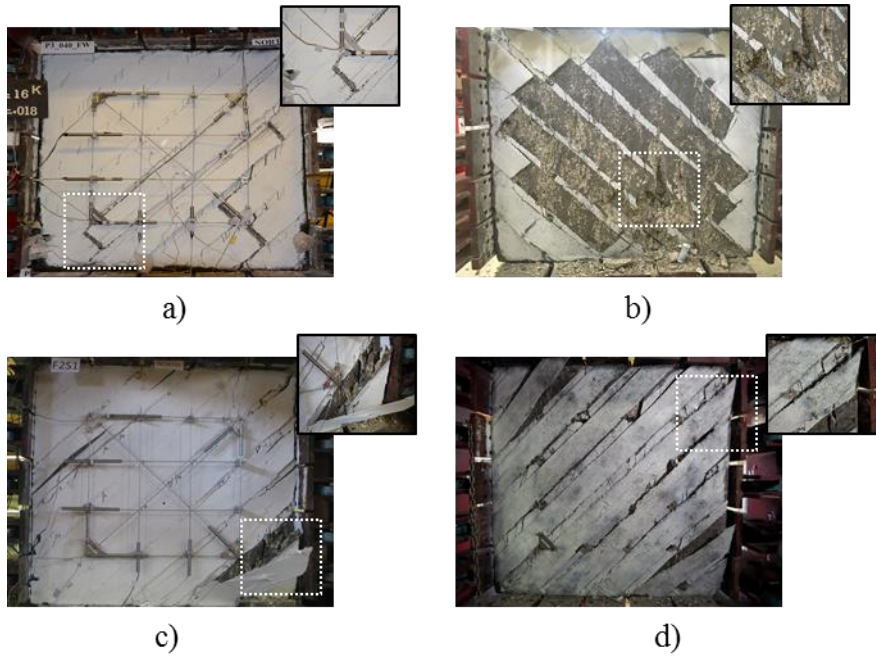
Fig. 15. Different failure modes of panel specimens, a) FRP debonding, b) Concrete crushing, c) FRP anchor failure, d) FRP rupture
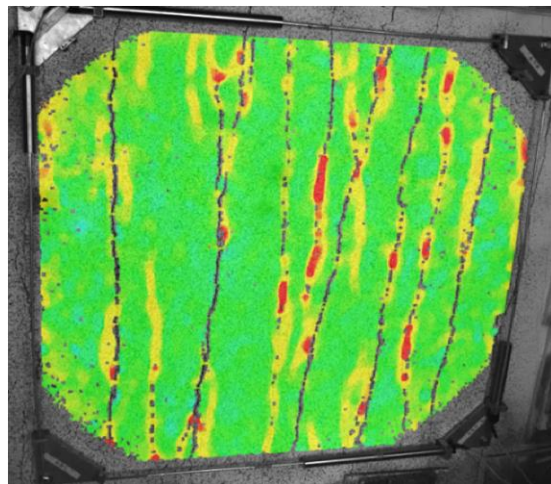

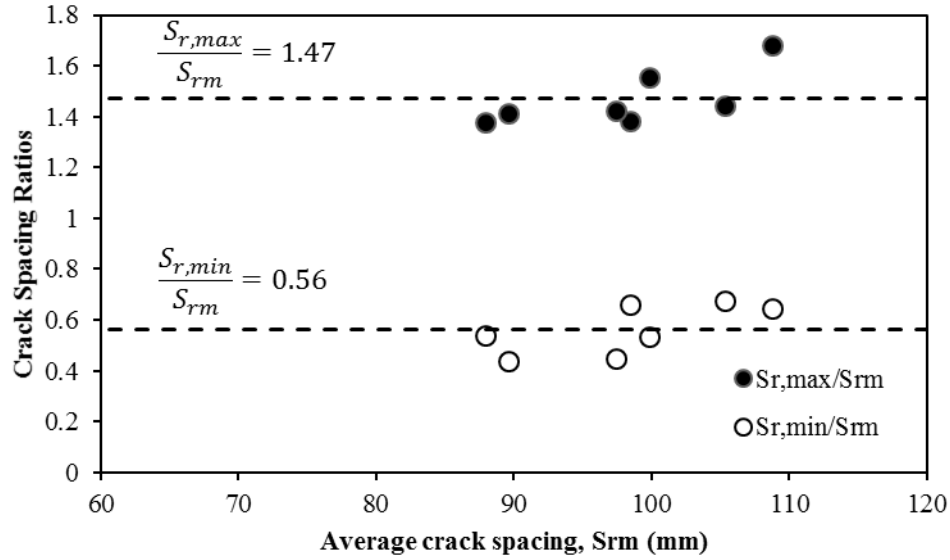**Fig. 16.** Full strain field in the direction of applied load of specimen at a specific load level

Fig. 17. Ratios of maximum and minimum to average crack spacing vs. average crack spacing in shear tests

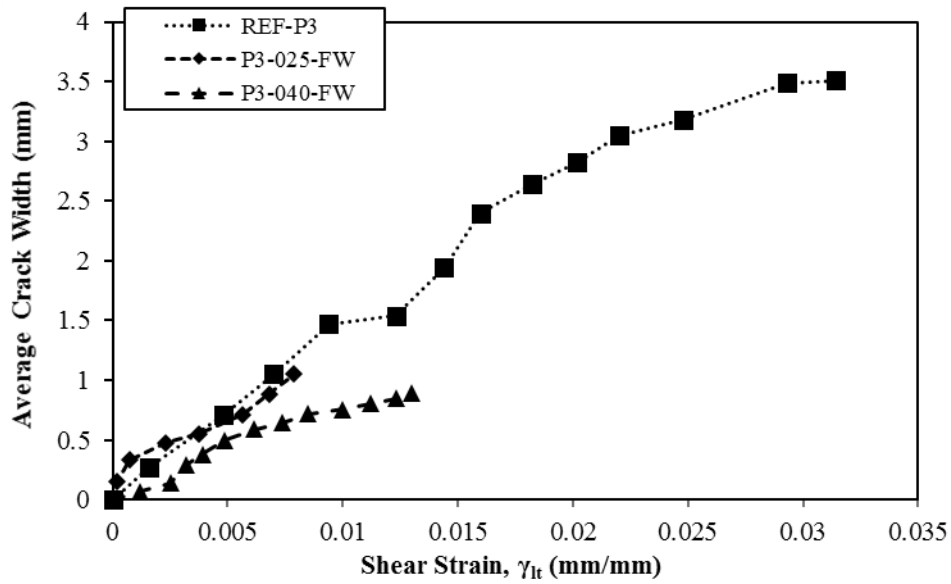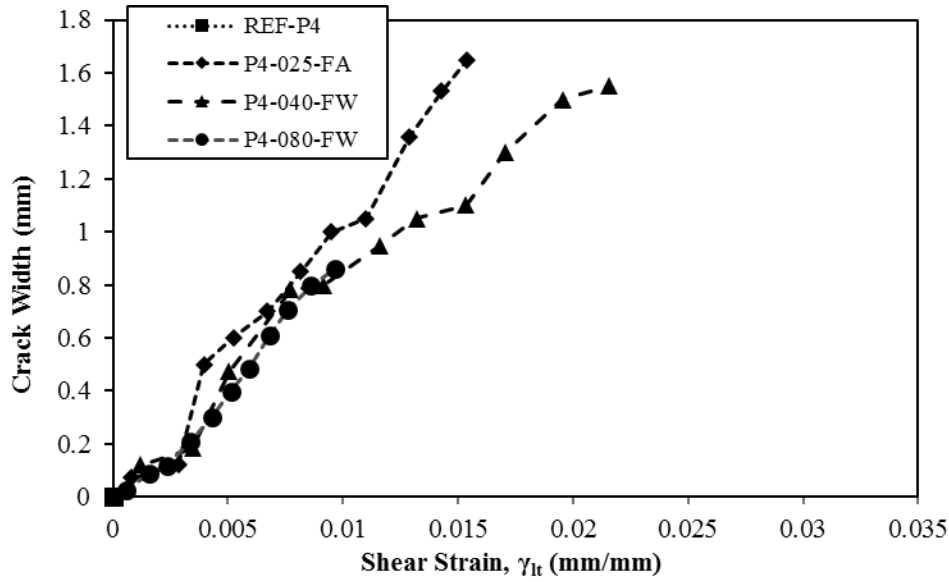**Fig. 18.** Average crack width comparison of panel series P3-FW and REF-P3

41

Fig. 19. Average crack width comparison of panel series P4-FW and P4-FA
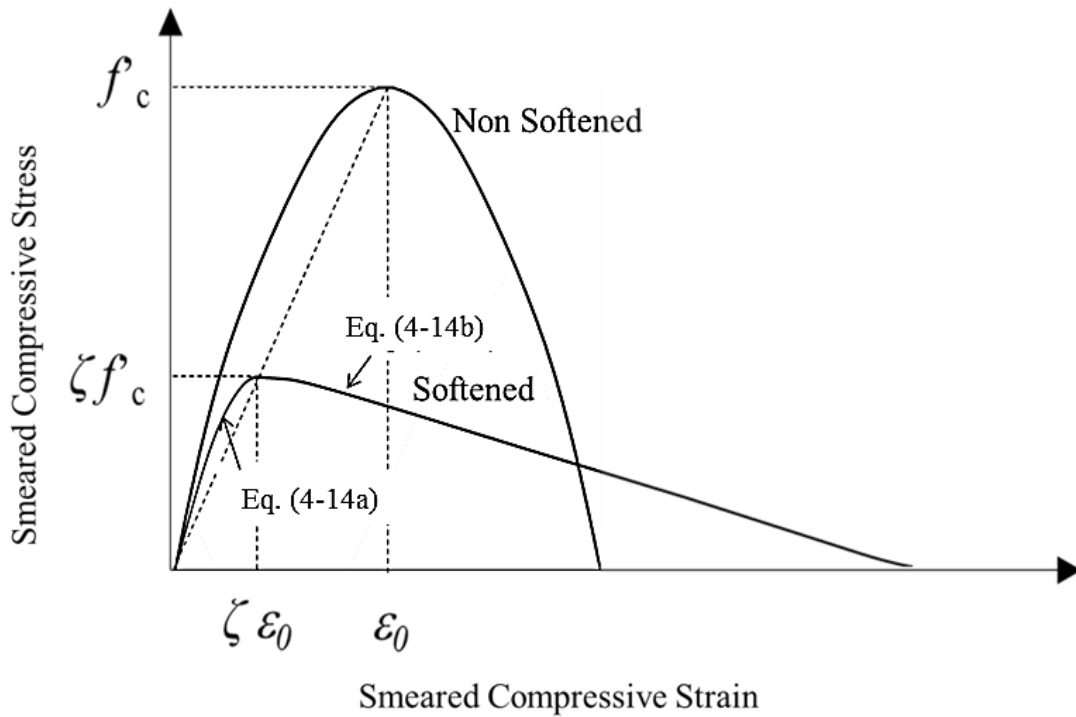

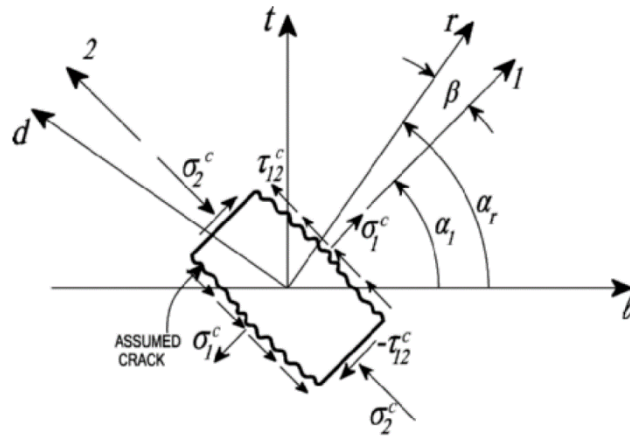Fig. 20. Monotonic Non-Softened and Softened Stress-Strain Curve [15]
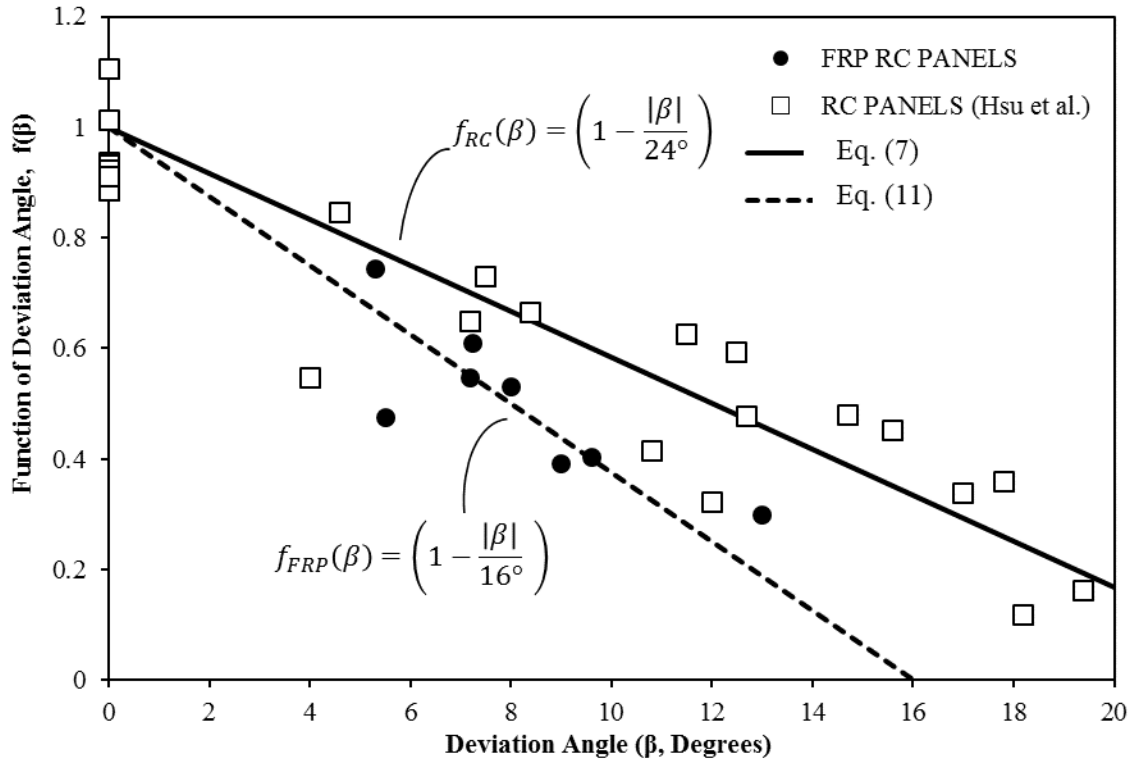
Fig. 21 Deviation Angle β [15]

Fig. 22 $f(\beta)$ versus β Relationships for RC and FRP Strengthened RC Panels

Table 1. Principal variables of test panel and material properties

43

Series	Specimen Name	Concrete	Steel in l direction			Steel in t direction			FRP in t direction	
		f'_c (MPa)	ρ_l (%)	f_{ly} (MPa)	E_{ls} (MPa)	ρ_t (%)	f_{ty} (MPa)	E_{ts} (MPa)	ρ_f (%)	E_f (MPa)
REF	REF-P3	53	0.76	462	190000	0.43	459	188000	-	-
	REF-P4	52	0.76	462	190000	0.76	462	190000	-	-
P3-FW	P3-025-FW	51	0.76	462	190000	0.43	459	188000	0.54	82700
	P3-040-FW	50	0.76	462	190000	0.43	459	188000	0.87	72400
P4-FW	P4-025-FW	45	0.76	462	190000	0.76	462	190000	0.54	82700
	P4-040-FW	52	0.76	462	190000	0.76	462	190000	0.87	72400
	P4-080-FW	54	0.76	462	190000	0.76	462	190000	1.74	72400
P4-SB	P4-040-SB	44	0.76	462	190000	0.76	462	190000	0.87	72400
P4-FA	P4-025-FA	52	0.76	462	190000	0.76	462	190000	0.54	82700
	P4-040-FA	52	0.76	462	190000	0.76	462	190000	0.87	72400

Table 2. Applied stresses and corresponding measured strains at peak load stage

Series	Panel	σ_{2m} (MPa)	σ_{1m} (MPa)	τ_{ltm} (MPa)	ε_{20} (mm/mm)	ε_{10} (mm/mm)	ε_{l0} (mm/mm)	ε_{t0} (mm/mm)	γ_{lt0} (mm/mm)
REF	REF-P3	-3.6	3.3	3.5	-0.000113	0.0228	0.0073	0.0172	0.0229
	REF-P4	-4.1	4.1	4.1	-0.000147	0.0219	0.0085	0.0117	0.0220
P3-FW	P3-025-FW	-4.2	3.7	4.0	-0.000164	0.0108	0.00632	0.00429	0.1089
	P3-040-FW	-4.7	4.1	4.4	-0.000241	0.0121	0.0059	0.0060	0.0122
P4-FW	P4-025-FW	-4.0	4.4	4.2	-0.000265	0.0067	0.0037	0.0024	0.0070
	P4-040-FW	-5.5	5.6	5.6	-0.000798	0.0166	0.0100	0.0050	0.0174
	P4-080-FW	-6.6	5.9	6.3	-0.000328	0.0165	0.0177	0.0065	0.0162
P4-SB	P4-040-SB	-3.9	4.7	4.3	-0.000114	0.0089	0.0047	0.0018	0.0091
P4-FA	P4-025-FA	-5.1	4.8	4.9	-0.000233	0.0162	0.0098	0.0045	0.0164
	P4-040-FA	-5.6	5.0	5.3	-0.000101	0.0187	0.0131	0.0042	0.0188

Table 3. Failure modes of test specimens

Panel	REF-P3	REF-P4	P3-025-FW	P3-040-FW	P4-025-FW	P4-040-FW	P4-080-FW	P4-040-SB	P4-025-FA	P4-040-FA
Failure Mode	Concrete crushing	Concrete crushing	FRP rupture	FRP rupture	FRP rupture	FRP rupture	Concrete crushing	FRP debonding	Anchor Failure/rupture	FRP rupture

Table 4. Experimental maximum, minimum and average crack spacing of panels at stabilized cracking stage

Specimen	No. of cracks	$S_{r,max}$ (mm)	$S_{r,min}$ (mm)	S_{rm} (mm)
REF-P3	10	151.89	71.37	105.35
REF-P4	8	121.16	47.49	87.95
P3-0250-FW	12	182.82	70.38	108.81
P3-040-FW	11	136.14	65.02	98.46
P4-025-FA	10	138.94	43.44	97.43
P4-040-FW	12	154.94	53.16	99.79
P4-080-FW	13	126.49	39.37	89.57

Table 5. Calculation of β and $f(\beta)$ for FRP Strengthened RC Panels

Specimen	ζ_{exp}	$f_c^{'}$ (Mpa)	$f(f_c^{'})$	$\bar{\varepsilon}_1$	$f(\bar{\varepsilon}_1)$	$\rho_f E_f$ (Mpa)	$f(FRP)$	$f(\beta)_{exp}$	$\beta°$
P3-025-FW	0.184	51	0.812	0.017	0.367	463.3	1.164	0.529	8.0
P3-040-FW	0.158	50	0.820	0.012	0.413	651.6	1.193	0.390	9.0
P4-025-FW	0.198	45	0.864	0.012	0.415	463.3	1.164	0.473	5.5
P4-040-FW	0.204	52	0.804	0.018	0.349	651.6	1.193	0.608	7.3
P4-080-FW	0.110	54	0.789	0.016	0.367	1259.7	1.269	0.298	13.0
P4-040-SB	0.190	44	0.874	0.010	0.452	651.6	1.193	0.402	9.6
P4-025-FA	0.184	52	0.804	0.017	0.359	463.3	1.164	0.547	7.2
P4-040-FA	0.200	52	0.804	0.029	0.280	651.6	1.193	0.744	5.3